Direct ab Initio Dynamics Study of the Unimolecular Reaction of CH_2FO

Qiong Luo and Qian Shu Li*

School of Science, Beijing Institute of Technology, Beijing 100081, P. R. China

Received: January 19, 2004; In Final Form: April 15, 2004

A direct ab initio dynamics study is carried out for three channels of the unimolecular reaction of fluoromethoxy, CH_2FO. The minimum energy paths (MEPs) of the three channels are computed with the MPW1K/6-31+G-(d,p) method. The geometries, harmonic vibrational frequencies, energies, and enthalpies of all stationary points are calculated at the MPW1K and QCISD levels of theory in conjunction with the 6-31+G(d,p) basis set. The energies of stationary points and the points along MEP for each channel are further refined by using single-point multilevel energy calculations. The rate constants are evaluated by means of the conventional transition state theory (TST), the canonical varitional transition state theory (CVT), and the canonical varitional transition state theory with small-curvature tunneling correction (CVT/SCT) in the temperature range of 200−2500 K. The fitted Arrhenius expressions of the calculated CVT/SCT rate constants are $k_1^{CVT/SCT}(T) = (1.26 \times 10^6)T^{2.19}e^{-7150.6/T}$ s^{-1}, $k_2^{CVT/SCT}(T) = (3.68 \times 10^2)T^{3.23}e^{-12327.7/T}$ s^{-1}, $k_3^{CVT/SCT}(T) = (9.97 \times 10^{-26})T^{10.90}e^{-3873.3/T}$ s^{-1} for the H elimination, HF elimination, and isomerization channels, respectively.

I. Introduction

Alkoxy radicals are known to be important intermediates in combustion and atmospheric chemistry. A great deal of work has been done on methoxy and chloroalkoxy radicals, but much less information is available on another halogen-substituted alkoxy radical, fluoromethoxy, CH_2FO.[1−4] Recently it has been realized that fluorocarbon and hydrofluorocarbon chemistry is important in a variety of areas including atmospheric chemistry, combustion suppression, and plasma etching in the microelectronics industry.[3] Therefore, investigation of the reactivity of CH_2FO may be of practical value as well as fundamental interest.

The CH_2FO radical is an intermediate in the oxidation of CH_3F (HFC-41).[4] Just as most alkoxy radicals, the primary atmospheric fate of CH_2FO is a unimolecular reaction, besides the reaction with O_2:[5]

$$CH_2FO + M \rightarrow \text{products} + M$$

As far as we know, there have been no accurate kinetic data on this reaction. However, there are a number of studies on some similar radicals. For example, Oguchi and co-workers have indicated that the CH_3O radical is mainly removed through the decomposition of the CH_3O radical by H atom elimination reaction at the temperatures above 500 K.[6] For $CCl_{3-x}F_xO$ radicals, theoretical investigation suggests that chlorine atom elimination processes dominate over fluorine atom dissociation processes.[7] In the study of the $O(^3P) + CHX_2$ (X = F, Cl) reactions, CHF_2O has been found to have four unimolecular production channels: H + CF_2O, CF_2OH, F + CHFO, and HF + FCO.[8] In addition, CH_2ClO elimination of HCl in a unimolecular reaction was characterized.[8−10]

In this study, we focus our interest on the potential pathways of the title reaction and the kinetic character of each pathway in the temperature range of 200−2500 K. Rayez et al. figured that the CH_2FO radical decomposes through two channels, the elimination of a fluorine atom or a hydrogen atom from CH_2-FO, and evaluated the barriers of the two possible decomposition pathways using the semiempirical method MNDO.[1] But the MNDO method generally is not very reliable for quantitative purposes. Indeed, in the present study, we cannot find the transition state for the F atom elimination path; instead, we locate a second-order saddle point with two imaginary frequencies of 4263i and 469i at the MPW1K/6-31+G(d,p) level of theory, in which one corresponds to the HF elimination and the other corresponds to the F elimination.

Therefore, in the present study, only three unimolecular channels of the title reaction are considered:

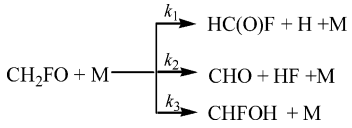

Their potential energy surface information is computed by using density functional theory and single-point multilevel energy calculations (HL). Their dynamical character is studied by means of the direct ab initio dynamics methods based on a canonical variational transition state theory (CVT) with the multidimensional centrifugal-dominant small-curvature semiclassical adiabatic ground-state tunneling (SCT) correction.

II. Calculation Methodology

Recent applications[11−13] have shown that the modified Perdew−Wang 1-parameter model for kinetics (MPW1K) method[11] can provide better predictions of energies and geometries than other hybrid Hartree−Fock-density functional (HF-DF) methods in some kinetics studies. And Truhlar and co-workers pointed out that the hybrid DFT results are much less sensitive to the basis set than the ab initio ones,[12] and they also emphasized the importance of diffuse functions. Then, in the present study, the geometries and frequencies of all stationary points (reactants, products, and the transition states) are

* Corresponding author. E-mail: qsli@bit.edu.cn. Fax: +86-10-68912665. Phone: +86-10-68912665.

10.1021/jp049736z CCC: $27.50
Published on Web 05/15/2004

optimized at the MPW1K level of theory with the 6-31+G-(d,p) basis set. Synchronously, to validate the reliability of the MPW1K method, the same calculations are performed by the quadratic configuration interaction theory with all single and double excitations (QCISD)[14] with the same basis set. To yield more reliable reaction enthalpy and barrier height, single-point calculations for all stationary points are further refined by means of single-point multilevel energy calculations (HL)[15] based on the optimized geometries at the MPW1K/6-31+G(d,p) and QCISD/6-31+G(d,p) levels of theory, denoted as HL//MPW1K and HL//QCISD, respectively. The HL method employs a combination of QCISD(T)[14] and MP2(FC)[16] methods, and can be expressed as

$$\begin{aligned} E_{\mathrm{HL}} = {} & E[\mathrm{QCISD(T)/cc\text{-}pVTZ}\ ] + \\ & (E[\mathrm{QCISD(T)/cc\text{-}pVTZ}\ ] - E[\mathrm{QCISD(T)/cc\text{-}pVDZ}\ ]) \times \\ & 0.46286 + E[\mathrm{MP2(FC)/cc\text{-}pVQZ}\ ] + \\ & (E[\mathrm{MP2(FC)/cc\text{-}pVQZ}\ ] - E[\mathrm{MP2(FC)/cc\text{-}pVTZ}\ ]) \times \\ & 0.69377 - E[\mathrm{MP2(FC)/cc\text{-}pVTZ}\ ] - \\ & (E[\mathrm{MP2(FC)/cc\text{-}pVTZ}\ ] - E[\mathrm{MP2(FC)/cc\text{-}pVDZ}\ ]) \times \\ & 0.46286 \end{aligned}$$

Here QCISD(T)/cc-pVTZ is referred to as the quadratic configuration interaction calculation including single and double substitutions with a triples contribution to the energy added,[14] using Dunning's correlation consistent polarized valence triple-ζ basis set.[17] The cc-pVDZ and cc-pVQZ stand for Dunning's correlation consistent polarized valence double-ξ basis set and polarized valence quadruple-ξ basis set,[17] respectively. MP2-(FC) denotes the second-order Moller−Plesset perturbation theory with frozen core approximation.[16] The information on the geometry, frequency, and energy provided by the MPW1K method agrees well with that obtained by the QCISD method. Considering efficiency and veracity synthetically, the minimum energy paths (MEPs) from $s = -1.50$ to 1.50 amu$^{1/2}$ bohr are done in the mass weighted Cartesian coordinate with a step size of 0.01 amu$^{1/2}$ bohr, using the intrinsic reaction coordinate (IRC) method[18] at the MPW1K/6-31+G(d,p) level of theory. At the selected points along the MEPs, the force constant matrixes as well as the harmonic vibrational frequencies are given at the same level. Furthermore, the energies of the selected points are recalculated by the HL method. All the electronic structure calculations are carried out with the Gaussian 98 program.[19]

By means of the VKLab Version 1.0 program,[20] the theoretical rate constants of the three channels of the title reaction are calculated by using the conventional transition state theory (TST), the canonical varitional transition state theory (CVT),[21−24] and canonical varitional transition state theory with small-curvature tunneling correction (CVT/SCT).[23] Within the framework of CVT, the generalized transition state rate constant, $k^{\mathrm{GT}}(T,s)$, can be calculated at the reaction coordinate s along the MEP at a fixed temperature; then the CVT rate constants are obtained by minimizing $k^{\mathrm{GT}}(T,s)$ along the MEP at the given temperature as follows

$$k^{\mathrm{CVT}}(T) = \min_{s} k^{\mathrm{GT}}(T,s)$$

in which

$$k^{\mathrm{GT}}(T,s) = \sigma \frac{k_{\mathrm{B}}T}{h} \frac{Q^{\mathrm{GT}}(T,s)}{Q^{\mathrm{R}}(T)} \mathrm{e}^{-V_{\mathrm{MEP}}(s)/k_{\mathrm{B}}T}$$

where σ is the reaction path multiplicity, k_{B} is Boltzmann's constant, h is Planck's constant, $\mathrm{Q^{GT}}(T,s)$ is the partition function of the generalized transition state at s, $Q^{\mathrm{R}}(T)$ is the reactant partition function per unit volume, and $V_{\mathrm{MEP}}(s)$ is the Born−Oppenheimer potential on the MEP.

Finally, the rate constant is

$$k(T) = \kappa(T) k^{\mathrm{CVT}}(T)$$

where $\kappa(T)$, transmission coefficient, can be calculated by the small-curvature tunneling (SCT)[23,25] method. And the quantum effects along the reaction coordinate can be included.

III. Results and Discussion

A. Stationary Points. Figure 1 displays the optimized geometries and the calculated geometric parameters of the equilibrium and transition states of the three channels along with the available experimental data.[26−28] For the products (HC(O)F, HCO, and HF), the theoretical bond lengths and bond angels are quite close to the experimental data with the largest deviation 0.034 Å (0.035 Å) for C−H and 5.6° (5.2°) for HOC of HCO, respectively, at the MPW1K/6-31+G(d,p) (QCISD/6-31+G-(d,p)) level of theory. When it comes to the reactant (CH_2FO) and its isomer (CHFOH), there are no experimental data. The structures provided by the two methods are in good agreement, and the differences are within 0.03 Å for bond lengths and 1° for bond angles. Consequently, the equilibrium geometries from the MPW1K/6-31+G(d,p) method agree well with the available experimental data, and are as accurate as those from the more expensive QCISD/6-31+G(d,p) method.

For transition states (TS_1, TS_2, and TS_3), the bond angles predicted at the two levels of theory are pretty close, whereas the lengths of the active bonds, C_1-H_5 of TS_1, and C_1-H_5, C_1-F_2, and H_5-F_2 of TS_2, as well as C_1-H_5 and O_3-H_5 of TS_3, calculated at the two methods are slightly different, respectively. For example, the active bond of TS_1, C_1-H_5, from the MPW1K/6-31+G(d,p) method is longer than that from the QCISD/6-31+G(d,p) method by 0.075 Å. It could be seen from Figure 1 that, except for the active bonds, the lengths of the other bonds of TS_1 are quantitatively similar to the corresponding bond of the product, HC(O)F. In view of TS_2 and TS_3, the same characteristic also appears, yet not as notable as TS_1. Therefore, TS_1 can be described as simple H−C bond rupture. In the case of TS_2, the geometry is best described as a 1,2 shift of F across the H_5-C_1 bond of CH_2O. Similar to population analysis for the stationary points (reactants, products, and transition states) of the reaction HXCO → CO + HX (X = F, Cl),[29] fluorine with a highly electronegative atom has a partial negative charge, attracting the H atom with a little positive charge in the CH_2FO molecule, which is consistent with the greater stability of $F^- + CH_2O^+$ compared to $F^+ + CH_2O^-$. Considering that the geometries of TS_3 and TS_2 are alike, TS_3 can also be described as a 1,2 shift of H across the O_3-C_1 bond of CHFO.

The harmonic vibrational frequencies and the zero-point energies of the equilibrium and transition states at the MPW1K/6-31+G(d,p) and QCISD/6-31+G(d,p) levels of theory as well as the available experimental data[27,28,30,31] are tabulated in Table 1. For the species HC(O)F, HCO, and HF, the computed frequencies from both levels are in good agreement with the experimental values, except that the frequencies of H−C stretch of HCO are overestimated by both methods with the discrepancy of about 10% as compared to the experimental value. The frequencies of CH_2FO and CHFOH and the real frequencies of the three transition states calculated by the two different methods are consistent. For each channel, the transition state has only

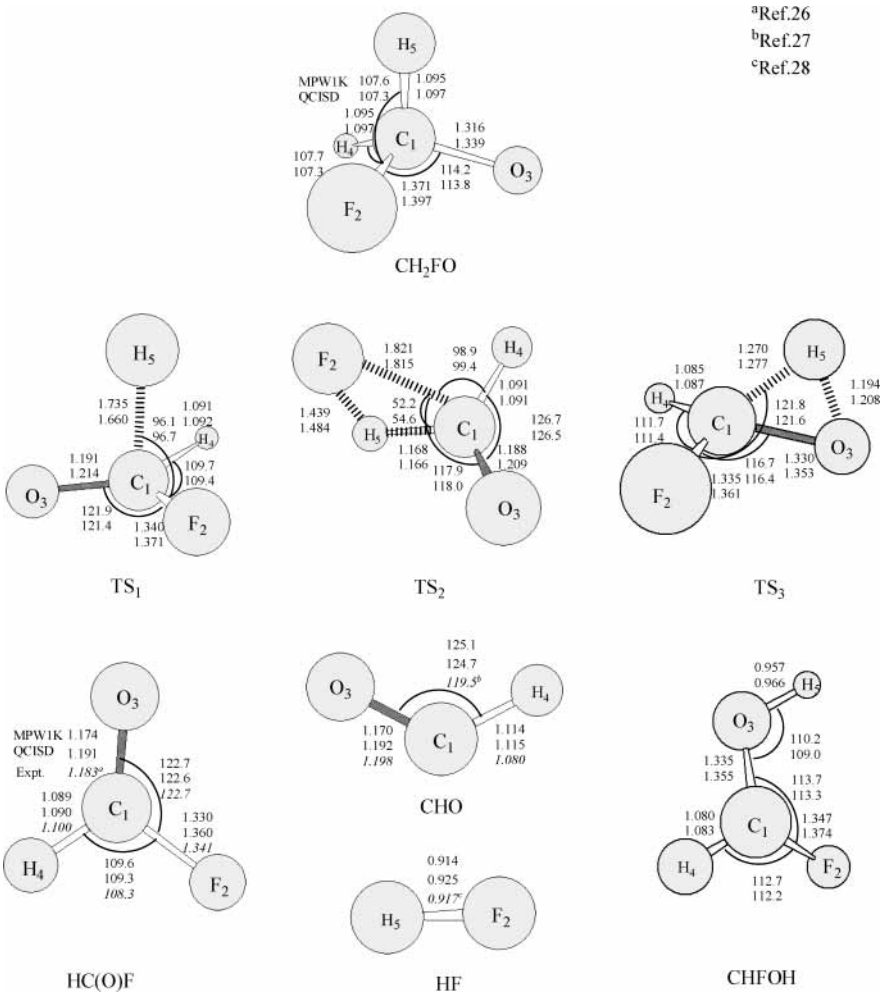

Figure 1. Optimized geometries of the stationary points of the title reaction.

TABLE 1: Harmonic Vibrational Frequencies (cm^{-1}) and Zero-Point Energies (kcal mol^{-1}) of the Reactant, Products, and Transition States, Using the Two Methods with the Same Basis Set 6-31+G (d,p)

species	methods	frequencies									ZPE
$CH_2FO(C_s)$	MPW1K	568	847	1080	1210	1216	1404	1428	3050	3104	19.88
	QCISD	541	847	1029	1150	1195	1394	1433	3080	3098	19.62
$CHFO(C_s)$	MPW1K	689	1078		1154	1419	1989		3223		13.65
	QCISD	654	1035		1078	1404	1887		3211		13.25
	exptl[a]	662.5	1011.0		1064.8	1342.5	1836.8		2981.0		
$HCO(C_s)$	MPW1K	1147	2038		2826						8.59
	QCISD	1152	1879		2804						8.34
	exptl[b]	1076.5	1858		2442						
$HF(C_s)$	MPW1K	4268									6.10
	QCISD	4135									5.91
	exptl[c]	4138.3									
$CH_2FO(C_1)$	MPW1K	364	569	978	1117	1241	1345	1431	3282	3975	20.45
	QCISD	376	550	1001	1063	1208	1311	1415	3258	3874	20.09
$TS_1(D_{\infty h})$	MPW1K	500	544	676	1102	1129	1388	1825	3181	1048i	14.79
	QCISD	556	581	660	1052	1113	1368	1706	3168	1319i	14.59
$TS_2(C_s)$	MPW1K	372	664	926	1064	1317	1799	2444	3169	808i	16.81
	QCISD	382	738	923	1061	1325	1671	2455	3158	850i	16.75
$TS_3(C_1)$	MPW1K	571	705	1046	1164	1316	1394	2507	3222	2139i	17.05
	QCISD	542	678	1042	1101	1250	1360	2448	3206	2181i	16.62

[a] Reference 30. [b] References 27 and 31. [c] Reference 28.

one imaginary frequency. The order of the value of imaginary frequency is $TS_3 > TS_1 > TS_2$ at both levels of theory, which suggests that the HF elimination channel has the broadest barrier width. Then it could be expected that the tunneling effect for the H elimination and isomerization channels seems more important than that for the HF elimination channel in computing the rate constants of the reaction.

The reaction energies (ΔV), the classical potential barriers ($V^{\ddagger}$), the vibrationally adiabatic ground-state potentials (V_a^G), and the reaction enthalpies (ΔH°_{298K}) are collected in Table 2. Note that the values of $V^{\ddagger}$and V_a^G are computed at the corresponding saddle points. The differences of the reaction enthalpies calculated at the MPW1K/6-31+G(d,p) and QCISD/6-31+G(d,p) levels of theory are 7.02 kcal mol^{-1} for the H

TABLE 2: Reaction Energetic Parameters (kcal mol^{-1}) at Different Levels of Theory

method	ΔV	$V^{\ddagger}$	V_a^G	ΔH°_{298K}
$CH_2FO + M \rightarrow CHFO + H + M$				
MPW1K/6-31+G(d,p)	23.92	30.04	24.94	19.08
QCISD/6-31+G(d,p)	17.04	27.77	22.74	12.06
HL//MPW1K	14.17	21.91	16.81	9.33
HL//QCISD	14.12	22.40	17.36	9.14
$CH_2FO + M \rightarrow CHO + HF + M$				
MPW1K/6-31+G(d,p)	8.37	39.50	36.42	5.07
QCISD/6-31+G(d,p)	−1.22	36.42	33.55	−4.72
HL//MPW1K	−3.84	32.54	29.46	−7.14
HL//QCISD	−3.93	32.53	29.66	−7.43
$CH_2FO + M \rightarrow CHFOH + M$				
MPW1K/6-31+G(d,p)	−3.70	37.57	34.74	−2.95
QCISD/6-31+G(d,p)	−3.92	38.61	35.60	−3.27
HL//MPW1K	−6.86	32.89	30.06	−6.11
HL//QCISD	−6.96	32.76	29.75	−6.31

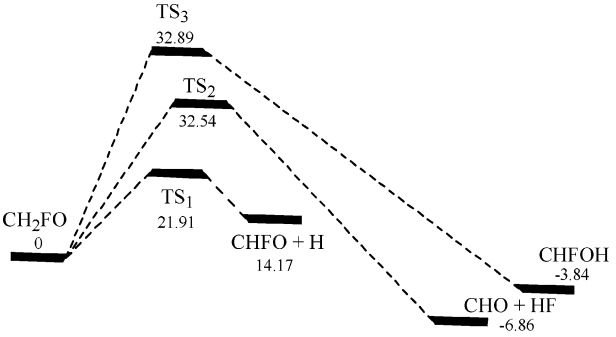

Figure 2. Energetic profile for the potential energy surface of the unimolecular reaction of CH_2FO at the HL//MPW1K level of theory.

elimination channel, 9.79 kcal mol^{-1} for the HF elimination channel, and 0.32 kcal mol^{-1} for the isomerization channel, whereas the differences at the HL//MPW1K and HL//QCISD decrease to 0.19, 0.29, and 0.20 kcal mol^{-1}, respectively. The same trend also appears for the vibrationally adiabatic ground-state potentials. This means that the MPW1K/6-31+G(d,p) level of theory can provide reasonable geometric information[11−13] but additional single-point HL calculations are needed to get accurate energetic information.

The energetic profile diagram (Figure 2) shows the HL//MPW1K energies of the three transition states and three sets of products relative to the ground-state energy of CH_2FO, arbitrarily taken as zero. It could be seen that the H elimination channel of the title reaction is endothermic while the HF elimination channel is exothermic, which is analogous to the thermochemical property of the H elimination channel and the HCl elimination channel of the decomposition of CH_2ClO.[32] However, the elimination of HCl from CH_2ClO involves a much lower barrier than the H elimination. But different from the isomerization reaction of CHF_2O and $CHCl_2O$, the isomerization channel in the present study is exothermic.

B. Reaction Path Properties. Figure 3 displays the variations of bond lengths with the IRC coordinates at the MPW1K/6-31+G(d,p) level of theory. For the H elimination channel, it is seen from Figure 3a that the change of the active C_1-H_5 bond (breaking) length is very steep after $s = -1.25$ amu$^{1/2}$ bohr. The C_1-O_3 bond length became shorter slowly up to about $s = 0.25$ amu$^{1/2}$ bohr, and later, the bond length shows nearly no change, which exhibits the proceeding of the C_1-O_3 single bond growing into a double bond. However, the changes of C_1-F_2 and C_1-H_4 bond lengths are not large. For the HF elimination channel, as shown in Figure 3b, the C_1-F_2 bond distance increases smoothly during the entire reaction process, and the

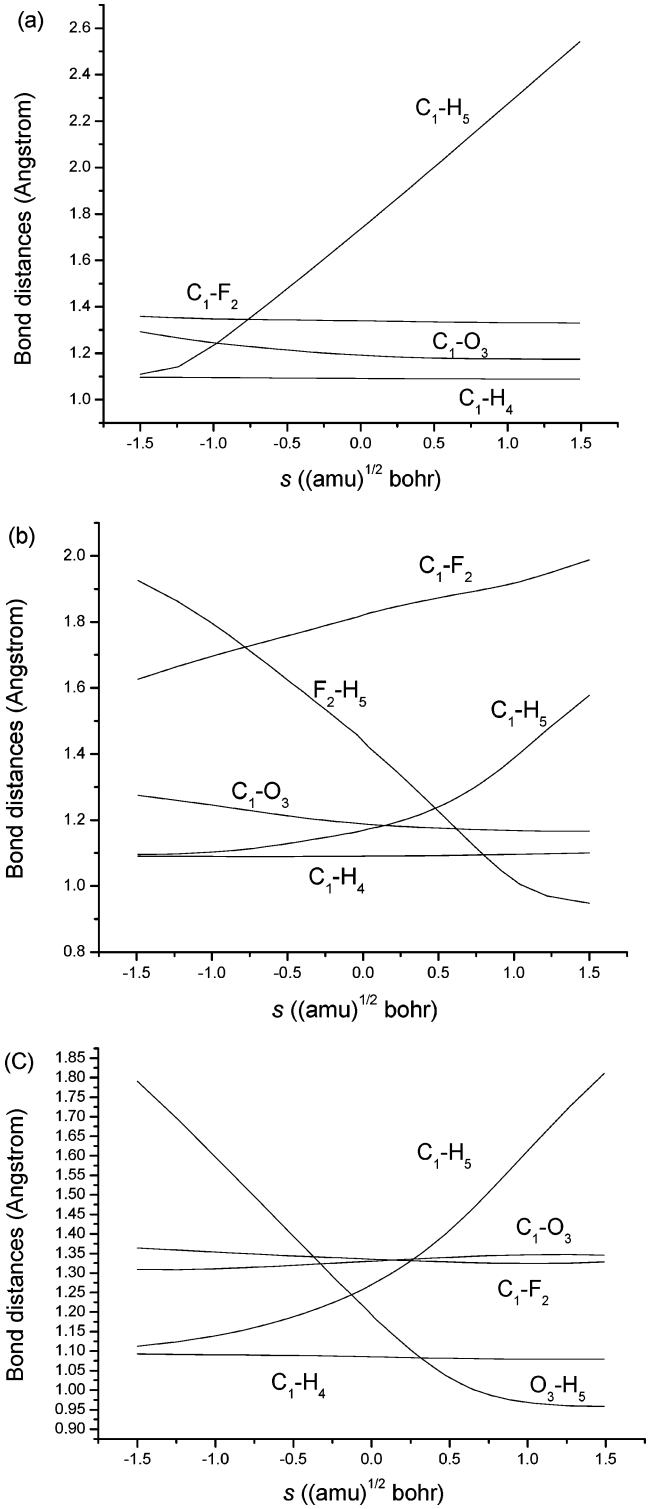

Figure 3. Variations of the bond distances of the reaction system with the IRC coordinate s at the MPW1K/6-31+G(d,p) level of theory: (a) the H elimination channel, (b) the HF elimination channel, and (c) the isomerization channel.

change of the C_1-H_5 bond length remains insensitive up to $s = -0.75$ amu$^{1/2}$ bohr and then increases rapidly afterward with the increase of the IRC coordinate. This confirms the conjecture that the geometry of TS_2 is a 1,2 shift of F across the H_5-C_1 bond of $C_1H_4H_5O_3$. The F_2-H_5 bond length, with the increase of the IRC coordinate, decreases smoothly to the H−F bond distance of 0.92 Å at $s = 1.4$ amu$^{1/2}$ bohr. The variations of the C_1-O_3 and C_1-H_4 bond distances are similar to those of the H elimination channel, respectively. In the case of the isomeriza-

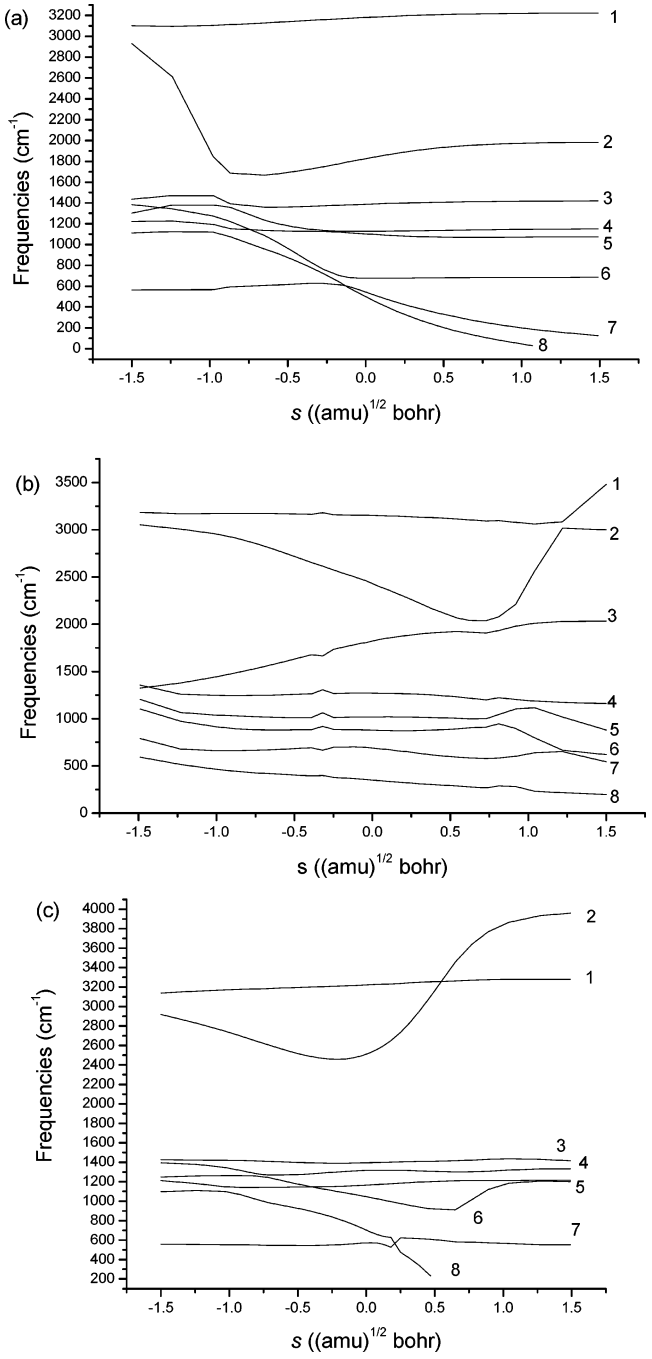

Figure 4. Variations of the generalized normal mode vibrational frequencies of the $CH_2FO + M$ reaction with the IRC coordinate s at the MPW1K/6-31+G(d,p) level of theory: (a) the H elimination channel, (b) the HF elimination channel, and (c) the isomerization channel.

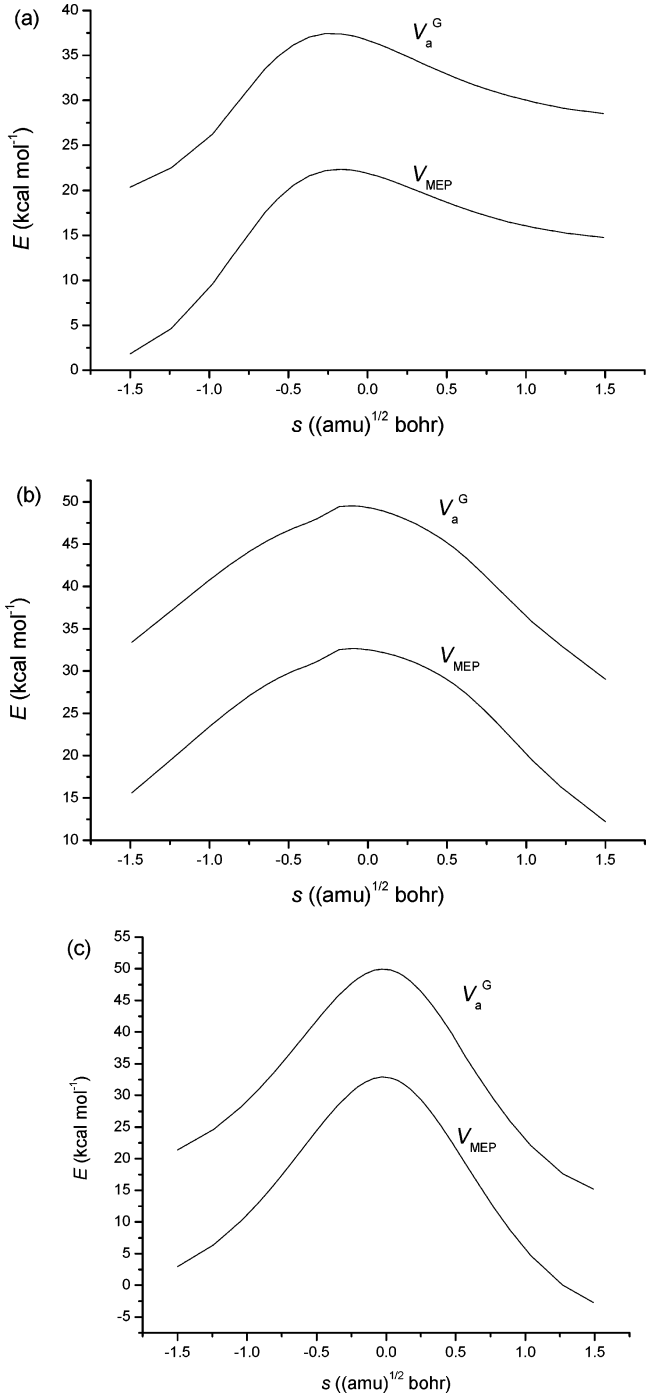

Figure 5. Variations of the classical potential energy (V_{MEP}) and the ground state vibrationally adiabatic potential energy (V_a^G) of the reaction system with the IRC coordinate s at the HL//MPW1K level of theory: (a) the H elimination channel, (b) the HF elimination channel, and (c) the isomerization channel.

tion channel (Figure 3c), the change of C_1-O_3, C_1-H_4, and C_1-F_2 bonds is negligible, and the curves of C_1-H_5 and O_3-H_5 bonds resemble those of C_1-H_5 and F_2-H_5 bonds of the HF elimination channel.

Figure 4 shows the variations of generalized normal mode vibrational frequencies along the MEPs of the three channels. In the negative and positive limits of s, the frequencies are respectively associated with the reactant, CH_2FO, and products, $HC(O)F + H$ for the H elimination channel (Figure 4a), $CHO + HF$ for the HF elimination channel (Figure 4b), and CHFOH for the isomerization channel (Figure 4c). In the vicinity of the transition states, when s approaches the saddle point, the frequency of the vibrational mode 2 drops and then increases slowly, as shown in Figure 4a, corresponding to a combination vibration of the C_1-O_3 stretching and C_1-H_5 stretching along the IRC path for the H elimination channel. For the HF elimination channel, vibrational mode 2 decreases rapidly after the transition state and rises quickly from the minimum, as shown in Figure 4b, corresponding to the combination vibration of the C_1-H_5 stretching and the H_5-F_2 stretching of TS_2. In Figure 4c, the curve of the vibrational mode 2 forms a vale near $s = 1.4$ amu$^{1/2}$ bohr, corresponding to the conversion of C−H stretching to H−O stretching. Obviously, vibrational mode 2 shown in Figure 4, panels a, b, and c, is the "reactive mode".

Figure 5 depicts the variations of the classical potential energy curves (V_{MEP}) and vibrationally adiabatic ground-state potential

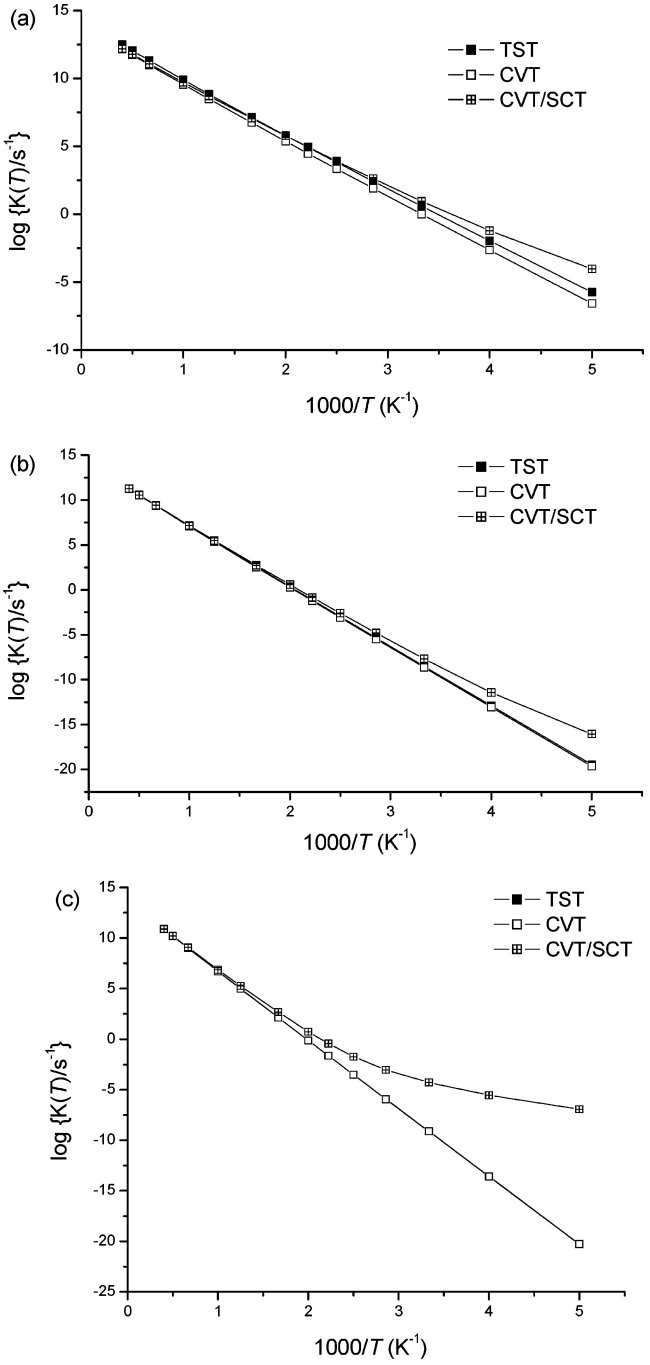

Figure 6. Fitted Arrhenius plots of the rate constants calculated at the HL//MPW1K level of theory of the title reaction vs $1000/T(K^{-1})$: (a) the H elimination channel, (b) the HF elimination channel, and (c) the isomerization channel.

energy curves (V_a^G) of the three channels with the increasing reaction coordinate *s* at the HL//MPW1K level of theory. The shapes of the classical potential energy curve and vibrationally adiabatic ground-state potential energy curve of each channel are similar, and show that all reaction channels undergo an elementary reaction process.

C. Rate Constant Calculations. The TST, CVT, and CVT/SCT rate constants are carried out for a temperature range from 200 to 2500 K on the MPW1K/6-31+G(d,p) MEPs with energies refined at the HL//MPW1K/6-31+G(d,p) level of theory. The fitted three-parameter Arrhenius expressions of the calculated CVT/SCT rate constants are $k_1^{CVT/SCT}(T) = (1.26 \times 10^6)T^{2.19}e^{-7150.6/T}$ s^{-1} for the H elimination channel, $k_2^{CVT/SCT}(T) = (3.68 \times 10^2)T^{3.23}e^{-12327.7/T}$ s^{-1} for the HF elimination channel, and $k_3^{CVT/SCT}(T) = (9.97 \times 10^{-26})T^{10.90}e^{-3873.3/T}$ s^{-1} for the isomerization channel. Figure 6 shows the Arrhenius plots vs the temperatures.

The curves of TST and CVT nearly overlap in panels a, b, and c of Figure 6, indicating that the variational effect on the calculation of rate constants is small and can be ignored for all three channels. For the H elimination channel, it could be found in Figure 6a that the curves of the CVT and CVT/SCT rate constants are quite close at a temperature above 1000 K, and with the decrease of the temperature both curves become separate gradually. The CVT/SCT rate constants are consistently larger than the CVT rate constants with the $k_1^{CVT/SCT}/k_1^{CVT}$ factor of 1.04 at 2500 K, and the corresponding factor increases to 357.9 at 200 K. In the case of the HF elimination channel, the tunneling effect is also crucial in the low-temperature area similar to the H elimination channel with the $k_2^{CVT/SCT}/k_2^{CVT}$ factor of 3884 at 200 K. As a proton transfer within the molecule, the tunneling effect of the isomerization channel is so remarkable that the $k_3^{CVT/SCT}/k_3^{CVT}$ factor is 2.17×10^{13} at 200 K.

In the present study, the rate constant k_1 is consistently larger than the rate constants k_2 and k_3, and the vaules of $k_1^{CVT/SCT}/k_2^{CVT/SCT}$ and $k_1^{CVT/SCT}/k_3^{CVT/SCT}$ increase with the decrease of the temperatures. From 200 to 2500 K, the ranges of the factor of $k_1^{CVT/SCT}/k_2^{CVT/SCT}$ and $k_1^{CVT/SCT}/k_3^{CVT/SCT}$ are about $1 \times 10^{12} \sim 9$ and $800 \sim 20$. When the temperature is under 600 K, the value of the factor of $k_2^{CVT/SCT}/k_3^{CVT/SCT}$ is less than 1, while it is over 1 when the temperature goes up to 600 K. As a result, the H elimination channel for the unimolecular reaction of CH_2FO is the dominating reaction in the whole temperature range.

IV. Summary

A direct ab initio dynamics study is carried out for the thermal rate constants of the three channels of the unimolecular reaction of CH_2FO. The calculated structural information at the MPW1K/6-31+G(d,p) and QCISD/6-31+G(d,p) levels of theory is similar r and in good agreement with the available experimental data. The computed reaction enthalpies of the three channels are quite close at the HL//MPW1K and HL//QCISD levels of theory. This suggests that the MPW1K/6-31+G(d,p) level of theory could provide reasonable geometric information. Furthermore, HL single-point energy refinement is needed to get more accurate energies.

The rate constants of the reaction are evaluated by using the TST, CVT, and CVT/SCT methods in the temperature range of 200−2500 K. The Arrhenius expression of the calculated CVT/SCT rate constants fitted at the HL//MPW1K level of theory for the H elimination channel is $k_1^{CVT/SCT}(T) = (1.26 \times 10^6)T^{2.19}$ $e^{-7150.6/T}$ s^{-1}, that for the HF elimination channel is $k_2^{CVT/SCT}(T) = (3.68 \times 10^2)T^{3.23}e^{-12327.7/T}$ s^{-1}, and that for the isomerization channel is $k_3^{CVT/SCT}(T) = (9.97 \times 10^{-26})T^{10.90}e^{-3873.3/T}$ s^{-1}. The results show that the rate constants for the three channels have positive temperature dependence in the temperature range 200−2500 K. The tunneling effect is important for the three channels in the low-temperature region, especially for the isomerization channel. The H elimination channel for the unimolecular reaction of CH_2FO is the dominating reaction in the whole temperature range, and in the low-temperature region, the HF elimination channel is the most subordinate channel in the present study, while the isomerization channel become most impossible when the temperature rises to 600 K.

Oguchi et al. pointed out that the potential barrier of H elimination from CH_3O was 24.3 kcal mol^{-1}, and indicated that CH_3O was mainly removed by this channel at temperatures

above 500 K.[6] Catoire et al. concluded that the potential barrier of HCl elimination from CH_2ClO was 18.9 kcal mol^{-1}, as well as the rate constant was 18×10^4 s^{-1} at 600 K, and suggested that the elimination of HCl from CH_2ClO was indeed a possible process at elevated temperatures.[32] In the present study, the calculated classical potential barrier of the H elimination from CH_2FO is 21.91 kcal mol^{-1} at the MPW1K/6-31+G(d,p) level of theory with the rate constant of 1.17×10^7 s^{-1} at 600 K. It seems reasonable to speculate that the unimolecular elimination of H should be considered as a possible fate of CH_2FO. Though there are no experimental dynamics data to confirm this surmise, these computational studies would be useful in providing further insight into the atmospheric chemistry of CH_2FO, and it could be expected that further experimental studies would be encouraged on the reaction.

Acknowledgment. This work was supported by the National Natural Science Foundation of China (20373007) and the Foundation for basic research by the Beijing Institute of Technology.

References and Notes

(1) Rayez, J. C.; Rayez, M. T.; Halvick, P.; Duguay, B.; Dannenberg, J. *J. Chem. Phys.* **1987**, *118*, 265.
(2) Dibble, T. S. *J. Mol. Struct.* **1999**, *67*−*71*, 485.
(3) Zachariah, M. R.; Westmoreland, P. R.; Burgess, D. R., Jr.; Tsang, W.; Melius, C. F. *J. Phys. Chem.* **1996**, *100*, 8737.
(4) Tuazon, E. C.; Atkinson, R. *J. Atmos. Chem.* **1993**, *17*, 179.
(5) Wallington, T. J.; Orlando, J. J.; Tyndall, G. S. *J. Phys. Chem.* **1995**, *99*, 9437.
(6) Oguchi, T.; Miyoshi, A.; Koshi, M.; Matsui, H. *Bull. Chem. Soc. Jpn.* **2000**, *73*, 53.
(7) Li, Z.; Francisco, J. S. *J. Am. Chem. Soc.* **1989**, *111*, 5660.
(8) Hou, H.; Wang, B.; Gu, Y. *J. Phys. Chem. A* **1999**, *103*, 8075.
(9) Wu, F.; Carr, R. W. *J. Phys. Chem. A* **2001**, *105*, 1423.
(10) Wu, F.; Carr, R. W. *J. Phys. Chem. A* **2002**, *106*, 5832.
(11) Lynch, B. J.; Fast, P. L.; Harris, M.; Truhlar, D. G. *J. Phys. Chem. A* **2000**, *104*, 4811.
(12) Lynch, B. J.; Truhlar, D. G. *J. Phys. Chem. A* **2001**, *105*, 2936.
(13) Lynch, B. J.; Truhlar, D. G. *J. Phys. Chem. A* **2002**, *106*, 842.
(14) Pople, J. A.; Head-Gordon, M.; Raghavachari, K. *J. Chem. Phys.* **1987**, *87*, 5968.
(15) Miller, J. A.; Klippenstein, S. J. *J. Phys. Chem. A* **2003**, *107*, 2680.
(16) Moller, C.; Plesst, M. S. *Phys. Rev.* **1934**, *46*, 618.
(17) Woon, D. E.; Dunning, T. H. *J. Chem. Phys.* **1993**, *98*, 1358.
(18) Gonzalez, C.; Schlegel, H. B. *J. Chem. Phys.* **1989**, *90*, 2154.
(19) Frisch, M. J.; Trucks, G. W.; Schlegel, H. B.; Scuseria, G. E.; Robb, M. A.; Cheeseman, J. R.; Zakrzewski, V. G.; Montgomery, J. A., Jr.; Stratmann, R. E.; Burant, J. C.; Dapprich, S.; Millam, J. M.; Daniels, A. D.; Kudin, K. N.; Strain, M. C.; Farkas, O.; Tomasi, J.; Barone, V.; Cossi, M.; Cammi, R.; Mennucci, B.; Pomelli, C.; Adamo, C.; Clifford, S.; Ochterski, J.; Petersson, G. A.; Ayala, P. Y.; Cui, Q.; Morokuma, K.; Malick, D. K.; Rabuck, A. D.; Raghavachari, K.; Foresman, J. B.; Cioslowski, J.; Ortiz, J. V.; Baboul, A. G.; Stefanov, B. B.; Liu, G.; Liashenko, A.; Piskorz, P.; Komaromi, I.; Gomperts, R.; Martin, R. L.; Fox, D. J.; Keith, T.; Al-Laham, M. A.; Peng, C. Y.; Nanayakkara, A.; Challacombe, M.; Gill, P. M. W.; Johnson, B.; Chen, W.; Wong, M. W.; Andres, J. L.; Gonzalez, C.; Head-Gordon, M.; Replogle, E. S.; Pople, J. A. *Gaussian98*; Gaussian, Inc.: Pittsburgh, PA, 1998.
(20) Zhang, S.; Truong, T. N. *J. Phys. Chem. A* **2001**, *105*, 2427.
(21) Truhlar, D. G.; Garrett, B. C. *J. Chem. Phys.* **1987**, *84*, 365.
(22) Truhlar, D. G.; Garrett, B. C. *Annu. Rev. Phys. Chem.* **1984**, *35*, 159.
(23) Truhlar, D. G.; Garrett, B. C.; Klippenstein, S. J. *J. Phys. Chem.* **1996**, *100*, 12771.
(24) Miller, W. H. *J. Am. Chem. Soc.* **1979**, *101*, 6810.
(25) Truong, T. N.; Truhlar, D. G. *J. Chem. Phys.* **1990**, *93*, 1761.
(26) LeBlanc, O. H., Jr.; Laurie, V. W.; Guinn, W. D. *J. Chem. Phys.* **1960**, *33*, 598.
(27) Herzberg, G. *Electronic spectra and electronic structure of polyatomic molecules*; Van Nostrand Reinhold: New York, 1966.
(28) Huber, K. P.; Herzberg, G., IV *Constants of Diatomic Molecules*; Van Nostrand Reinhold Co.: New York, 1979.
(29) Anand, S.; Schlegel, H. B. *J. Phys. Chem. A* **2002**, *106*, 11623.
(30) Choi, Y. S.; Moore, C. B. *J. Chem. Phys.* **1995**, *103*, 9981.
(31) Pettersson, M.; Khriachtchev, L.; Jolkkonen, S.; Rasanen, M. *J. Phys. Chem. A* **1999**, *103*, 9154.
(32) Catoire, V.; Lesclaux, R.; Lightfoot, P. D.; Rayez, M.-T. *J. Phys. Chem.* **1994**, *98*, 2889.